Porous Cu Nanowire Aerosponges from One-Step Assembly and their Applications in Heat Dissipation

Sung Mi Jung, Daniel J. Preston, Hyun Young Jung, Zhengtao Deng, Evelyn N. Wang, and Jing Kong**

Porous metals have important technological potential since they offer a unique combination of high conductivity, high surface area, and light weight properties into one material system. They have a wide range of potential applications including thermal management,[1] energy absorption,[2] catalysis, sensing, or filtration at high temperatures,[3] energy generation,[4] and/or storage,[5] lightweight optics,[6–9] vibration/sound absorption, etc. Despite the significant need for these materials, at present, there are only limited methods to obtain them, such as direct assembly from metal nanoparticles,[10–13] combustion synthesis,[14–18] electroplating (or electroless-plating) on fabricated microtemplates,[19–21] which are complicated and costly in manufacturing, and some of the processes are toxic and involve safety concerns. As a result, currently porous metals are only used in limited situations in advanced technology/manufacturing, or in aerospace applications where manufacturing cost and volume is not an important consideration.[14]

During the past few years, we developed a general methodology to produce highly porous aerogel structures from a variety of materials.[22] The method is based on shape anisotropy, such that in a solution dispersed with anisotropic nanomaterials (either 1D nanotubes, nanowires, or 2D nanosheets), these nano-objects can assemble into a bulk 3D network as the concentration of the solution increases (either by solvent evaporation,[22] or by nanowires directly grow out from the solution.[23] This method, because it is applicable to any type of nanowire or nanosheet materials, is applied in this work to develop a porous bulk 3D copper nanowire (CuNW) aerosponge from an interconnected CuNW hydrogel network formation during in situ nanowire synthesis. The process is very simple and low cost, the CuNW networks are assembled without specific crosslinking agent[24] but with extraordinary properties. Furthermore, it was also found that CuNW aerosponges with different porosities and density distributions and different electrical and mechanical properties can be obtained just by tuning the initial composition and concentration of the reaction precursor, and the growth time and temperature for the synthesis process, making the method flexible for specific needs in various applications.[25–31] One such application demonstrated in the present work is low-density high-performance wicks for fluid transport in heat pipes and other two-phase thermal management devices.

Figure 1a–e shows the in situ CuNW hydrogel network formation and the nanowire sponge production process. A homogeneous precursor aqueous suspension composed of (NaOH:C u$(SO_4)_2$:ethylenediame:Hydrazine) is initially prepared by ultrasonciation (Figure 1a), and the suspension is transferred to a glass/Teflon vessel and heated in an oil bath at various synthesis temperatures (50–85 °C) and for certain period of reaction time (30 min to 5 h). Metallic copper is formed by the reductive conversion from Cu^{2+} (Equation (1)) in the solution, and nanowires start to grow out (Figure 1b), as a result the solution changed to pinkish color.[32] During the reaction, as the CuNWs increase in length and concentration (Figure 1c,d), they start to interconnect with each other (Figure 1c schematic). As time goes on, the nanowires are self-assembled into an interconnected CuNW 3D network and a nanowire hydrogel forms after a reaction time of 20 min (Figure 1d). Interestingly, the as-prepared nanowire hydrogel floats on top of the solution (Figure 1d), presumably due to the entrapped gases generated (Equation (1)) among the nanowires. After the synthesis, the in situ CuNW hydrogel network is washed with an excess DI water/hydrazine solution several times to prevent Cu oxidation (Figure 1f) and subsequently the resultant hydrogel is transferred into aerosponges by freeze-drying as shown in Figure 1g (we also compared the CuNW networks via different drying methods in Figure S1, Supporting Information) and Various shapes and thicknesses of the bulk aerosponges can be produced by using different shaped/sized reaction containers and different amount of reaction solutions. Flexible, bendable, rollable, and semitrasparent large-area CuNW aerosponges are shown in Figure 1h–j, respectively (see Figures S2 and S3 for the X-ray diffraction and X-ray photoelectron spectroscopy results of Cu nanowire aerosponges in the Supporting Information). The CuNW aerosponges obtained from this method are highly porous (porosity: 99.95%) and have ultralong Cu nanowires in the network (Figure 1k; Figure S5 (Supporting Information))

Dr. S. M. Jung, Prof. J. Kong
Department of Electrical Engineering
and Computer Science
Massachusetts Institute of Technology
Cambridge, MA 02139, USA
E-mail: sungmij@mit.edu; jingkong@mit.edu
D. J. Preston, Prof. E. N. Wang
Department of Mechanical Engineering
Massachusetts Institute of Technology
Cambridge, MA 02139, USA
Prof. H. Y. Jung
Department of Energy Engineering
Gyeongnam National University of Science and Technology
Jinju 52725, South Korea
Prof. Z. Deng
College of Engineering and Applied Sciences
Nanjing University
Nanjing, Jiangsu 210093, P. R. China

DOI: 10.1002/adma.201504774

ADVANCED MATERIALS
www.advmat.de

www.MaterialsViews.com

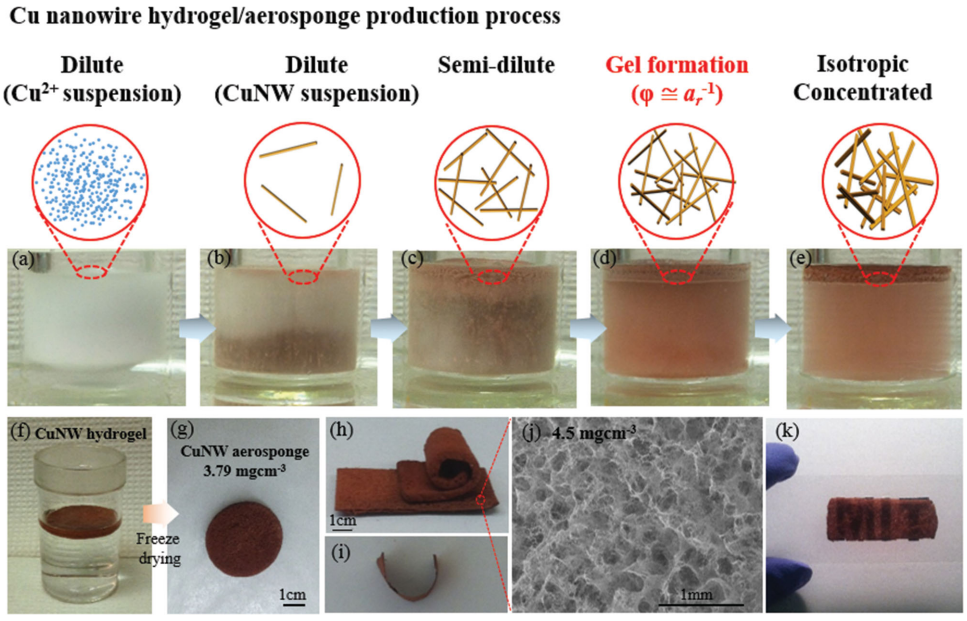

Figure 1. Cu nanowire hydrogel/aerosponge production process. a–e) The in situ CuNW network formation process. a) Cu precursor suspension soaked in oil bath, b) the initial step of CuNW synthesis by the reductive conversion of Cu^{2+}(dilute concentration regime of the CuNW suspension), c) the initial interconnection step of the synthesized nanowires (semidilute), and d) the in situ CuNW network formation step by self-assembly at reaction time of 20 min (the transition between semidilute and isotropic concentrated regime), e) more concentrated hydrogel at 30 min (isotropic concentrated regime). f) The in situ CuNW hydrogel after washing. g) Optical image of the CuNW aerosponge from (f) by freeze-drying, h,i) optical images of the flexible, bendable, and rollable aerosponges, j) low magnification SEM (Scanning Electron Microscope) image of porous surface and the 3D nanowire network structure of the aerosponge h). k) Optical image of a semitransparent thin aerosponge.

$$2Cu^{2+} + N_2H_4 + 4OH^- \rightarrow 2Cu + N_2 + 4H_2O \quad (1)$$

It is worth pointing out that the reaction in Equation (1) has been used to synthesis Cu nanowires with high yield previously.[32] In fact, Cu nanowire aerogel was also reported by redispersing the Cu nanowires synthesized with the aforementioned method[32] and followed by freeze-casting to make a loosely bonded 3D bulk via freezing of the suspension and subsequently removing the frozen liquid by sublimation using a freeze dryer.[33] But the significant element distinguishing our current work with the previous[32,33] lies in the fact that the nanowires directly assemble into a highly porous, interconnected, and robust 3D hydrogel network in situ during the synthesis. No crosslinking agents or supporting templates were needed. In order to achieve this, the optimized conditions identified for this work (see below) are quite different from reported previously.[32] Such essential difference in the preparation has lead to much superior properties of the resulting networks. First, because the nanowires directly assemble into the network without the redispersion step (during which the nanowires very likely are cut short or damaged due to the sonication), the entanglement between long nanowires entails excellent electrical and mechanical contact; second, because the nanowire hydrogels are formed first before they are transformed into aerosponges by freeze drying, the size, shape of the hydrogels/aerosponges maintain their integrity throughout the process even at extremely low densities.

In order to obtain ultrafine and highly porous in situ 3D networks, we tuned the porosity of the aerosponge via variation of reaction temperature, the concentration of the precursor suspension, and reaction time (see the Experimental Methods section in the Supporting Information). As a first step, the influence of reaction temperature is investigated within a range of 50–85 °C. As can be seen in the representative examples of **Figure 2**a–c, it was found with synthesis temperatures of 60, 70, and 80 °C, the resultant Cu nanowire aerosponges show highly porous and ultrafine nanowire network without bundles. Comparing within these synthesis temperatures, the porosities of these aerosponges look similar from the SEM (scanning electron microscopy) images in Figure 2a–c but the aerosponge synthesized at higher temperatures (Figure 2c) show much fewer Cu disks as impurities than the ones at lower temperatures (Figure 2a,b), as a result, the aerosponge synthesized at higher temperatures have lower densities (Figure 2g). A density of 4.5 mg cm^{-3} was obtained for the 80 °C sample, it is ≈22% less than the one synthesized at 60 °C with otherwise the same conditions, presumably the Cu disks contribute to the higher density in those samples. For the CuNW network obtained at temperatures above 80 °C, because the gas bubble generation rate (Equation (1) is too large, the resulting bulk structure is no longer uniform. Furthermore, slight oxidation of the nanowires on the top surface (exposed to air) was observed at these temperatures. Therefore, 80 °C was identified as the optimum synthesis temperature. As a second step, NaOH concentration was experimented (from 11 to 18 M). The results of 13 M (Figure 2d), 16 M (Figure 2c), and 18 M (Figure 2e) at the temperature of 80 °C are presented. The aerosponges from 16 to 18 M NaOH exhibited ultralong nanowire networks with uniform nanowire

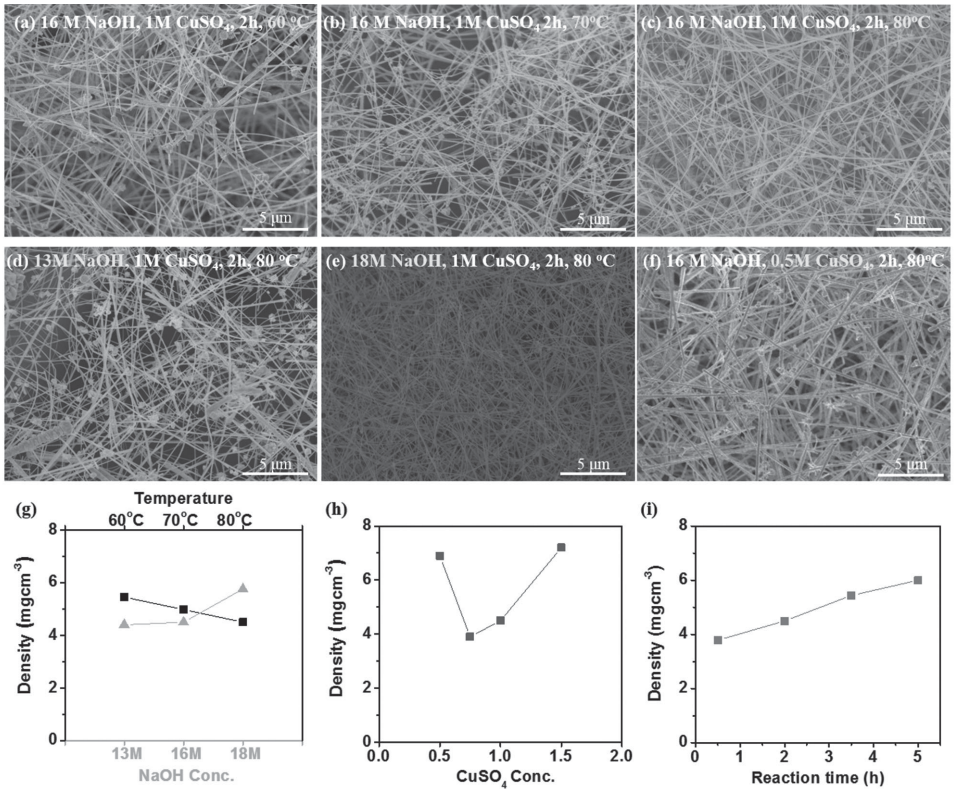

Figure 2. Optimization of the CuNW aerosponge synthesis condition. a–c) SEM images of the ultrafine and highly porous aerosponges synthesized with 16 M NaOH concentration, 1 M $CuSO_4$ concentration, 2 h reaction time, and different reaction temperatures: a) 60 °C, b) 70 °C, c) 80 °C. d,e) SEM images of the resulting aerogels synthesized with 80 °C reaction temperature, 1 M $CuSO_4$ concentration, 2 h reaction time and different NaOH concentrations: d) 13 M, e) 18 M. f) SEM image of the resulting aerosponge with 16 M NaOH concentration, 80 °C reaction temperature, 2 h reaction time but 0.5 M $CuSO_4$ concentration. g) The dependence of the Cu NW aerosponge density on the synthesis temperature or NaOH concentration, h) the dependence of density on $CuSO_4$ concentration (0.5, 0.75, 1, 1.5 M), i) the dependence of density on the reaction time (0.5, 2, 3.5, 5 h).

diameters ranging from 70 to 90 nm and much fewer Cu disks (Figure 2c,e), while the Cu nanowire network obtained at 13 M NaOH contains many Cu disks impurities and the nanowire diameters were un-uniform (Figure 2d). Comparing between the 16 and 18 M NaOH results, the density of the 18 M sample is ≈22% higher than the 16 M sample, as can be seen from the SEM images in Figure 2c versus e, and the plot in Figure 2g. The porosity is reduced and the density of the aerosponges increases as the NaOH concentration increases (Figure 2g). Presumably, with higher NaOH concentration, more nucleation occurs at the initial stage of the $Cu(^{2+})$ reduction, leading to denser nanowires in the structure (at a too low (11 M or 13 M) NaOH concentration, a noticeable amount of them did not result in Cu nanowires but Cu disks instead). As a third step, the concentration of the $CuSO_4$ solution was also experimented (from 0.25 to 1.5 M). At 0.25 M $CuSO_4$, a CuNW network could not form because Cu ion concentration was not high enough to form the interconnected CuNW network. Figure 2f and Figure S6a (Supporting Information) show the SEM image of the aerosponge obtained with 0.5 M $CuSO_4$, which is half of the concentration used in the condition for Figure 2c and Figure S6b (Supporting Information) (all the other conditions were the same). Comparing between Figure 2c,f, it can be seen that the Cu nanowires in Figure 2f have slightly higher local density but with apparently shorter lengths. As a result, the density of the aerosponge synthesized with 0.5 M $CuSO_4$ concentration is more than 50% higher (6.9 mg cm^{-3} vs 4.5 mg cm^{-3}, shown in Figure 2h) than the one synthesized with 1 M $CuSO_4$. Further characterizations also reveal that the aerosponge synthesized at 1 M $CuSO_4$ has better electrical/mechanical properties. Therefore, from these investigations, it is concluded that the optimal synthesis condition at 16 M NaOH concentration, 1 M $CuSO_4$ concentration, and 80 °C temperature favors aerosponge structure with high porosity, high purity, and robust nanowire network. A study of reaction time was carried out based on this optimized condition, from the reaction starting point to 15 h. The density of the resulting networks are plotted versus the reaction time in Figure 2i. It can be seen that as time goes on from 30 min to 5 h, the densities increased from 3.79 to 6 mg cm^{-3}. It is noticed that the aerosponge could not be produced if the reaction time is longer than 15 h because the Cu nanowires were oxidized after 15 h and then the hydrogel network was broken. For reaction time shorter than 30 min, the resulting network density is very low, but the bulk structure is not mechanically robust. And for reaction time in between 5 and 15 h, because there were too many gas bubble generated, the bulk structure was not uniform. Therefore for this study we have limited the reaction time to be within 30 min to 5 h.

As we have found previously, the nanowire gel formation concentration depends on the aspect ratio of the nanowires.[22] In

the present work, since the in situ CuNW hydrogel was obtained directly from the Cu nanowire synthesis without any dispersion of the nanowires, ultralong nanowires with lengths up to several hundred micrometers remain in the gel network, giving rise to a very high aspect ratio. Therefore, these in situ assembled networks could form at a much lower concentration and the resulting aerosponge has a density as low as 3.79 mg cm^{-3} which is 2300 time lighter than bulk copper (8.96 g cm^{-3}) and 240 time lighter than styrofoam (0.906 g cm^{-3}), while still remain as an integral and robust 3D bulk with excellent electrical and mechanical properties. This feature marks the distinguishing characteristic of the aerosponges made in this work when comparing to other porous structures reported previously.

The excellent structure of these Cu nanowire aerosponge network resulted in extraordinary properties as shown in the electrical and mechanical characterizations (**Table 1** and **Figure 3**). Figure 3a compares the electrical conductivities of several porous material systems. For densities as low as only three to six times as that of air (or below), our bulk 3D Cu nanowire aerosponge network shows electrical conductivities as high as 116 S cm^{-1}, which is so far the highest among all reported conductive porous structures. As a further comparison, the relative conductivity is plotted against relative density to separate the influence of intrinsic material characteristic (Figure 3b). For Cu nanowire aerogel made from freeze casting of the redispersed nanowire suspension[33] at a density of 7.69 mg cm^{-3}, the electrical conductivity is 129 times lower than our CuNW aerosponge of similar density of 7.5 mg cm^{-3} made in this work. Such sharp difference in conductivity can be attribute to the long length of the nanowires without being cut short or damaged by sonication, the robust contact and intertwining entanglement between the nanowires. Interestingly, power-law scaling was found for both material systems, but with very different exponents: an exponent of 3.2 was found for this work. Previously it was predicted that the exponent for

Table 1. The electrical conductivities of CuNW aerosponges with different densities obtained from different reaction conditions of NaOH and $CuSO_4$ concentration and reaction time and temperature.

NaOH Conc. [M]	$CuSO_4$ Conc. [M]	Reaction time [h]	Temp. [°C]	Density [mg cm^{-3}]	Conductivity [S cm^{-1}]
16	1	0.5	80	3.79	13
13	1	2	80	4.4	18
16	1	2	80	4.5	28
18	1	2	80	5.76	57
16	1	5	80	6	60
16	0.5	2	80	6.9	95
18	1	5	80	7.5	116

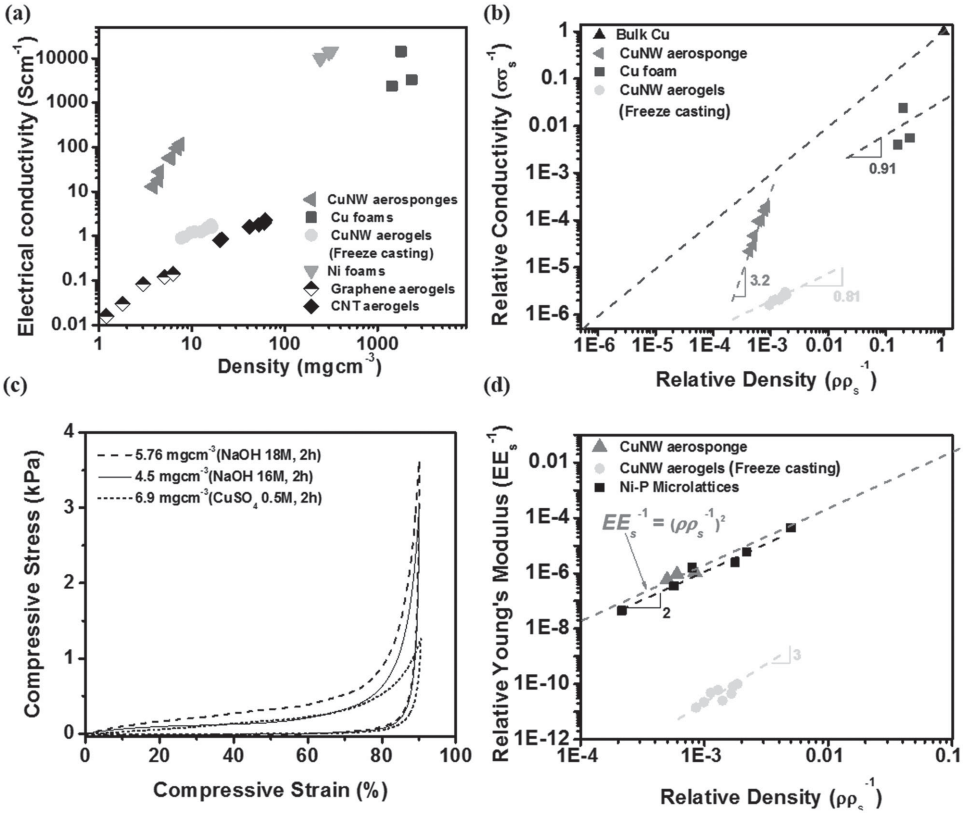

Figure 3. Electrical and mechanical properties of the CuNW aerosponges. a) The conductivity vs density (absolute not relative). b) The relationship between relative electrical conductivity and relative density of CuNW aerosponges compared to other porous metals. c) Compressive stress/strain test for the aerosponges with different densities of 5.76 mg cm^{-3} (NaOH 18 M, 1 M $CuSO_4$, 2 h, 80 °C), 4.5 mg cm^{-3} (NaOH 16 M, 1 M $CuSO_4$, 2 h, 80 °C), 6.9 mg cm^{-3}. d) The relationship between relative Young's modulus and density of CuNW aerosponges, together with data from the literature as comparison.

percolative networks with random, isotropic components would be ≈1.3 in 2D systems and ≈2.0 in 3D systems,[34] though the values of the exponent reported for 3D systems vary greatly, from 1.5 to 2.36.[35] For anisotropic components, it has been predicted that exponents larger (or smaller) than those values will arise depending on the direction of the measurement.[36] In recent years, significant efforts have been made in studying transparent conductive films from carbon nanotube or metallic nanowires. For such 2D percolative networks composed of these anisotropic systems, exponents of 1.75 has been reported for junction resistance dominated network,[37] larger than the predicted value with isotropic components. Clearly the conductivity of individual nanowire component and the good contact between them contribute favorably to the exponents of 3.2 observed in our 3D Cu nanowire percolative network, and this result calls for further modeling efforts to study such systems in the future.

In addition to the extraordinary electrical properties, mechanical tests on our CuNW aerosponge also revealed outstanding characteristics. Mechanical robustness plays critical importance for the practical applications of such low density, high surface area porous materials. Figure 3c shows the results of compressive tests of CuNW aerosponge with several densities (all synthesized for 2 h reaction time). These flexible and bendable aerosponges showed elastic behavior even at compressive strains as high as 90%. They can be compressed greatly but then restore when the pressure was released, and this can repeat many times without fracture (we investigated the morphology of CuNW network before and after compression in Figure S7 in the Supporting Information). When comparing the 4.5 mg cm^{-3} sample (synthesized under optimal condition for 2 h) with the 6.9 mg cm^{-3} sample (synthesized with 0.5 M $CuSO_4$ and otherwise the same condition as the optimal one for 2 h), it can be seen that even the 6.9 mg cm^{-3} sample has higher density, its Young's modulus is lower than the 4.5 mg cm^{-3} sample by 300 Pa. This can be understood from the fact that even though the 6.9 mg cm^{-3} sample has more Cu nanowires, but from the SEM images it was observed that the nanowires have shorter length, therefore it is easier for this sample to be compressed. On the other hand, when comparing the 5.76 mg cm^{-3} sample (synthesized with 18 M NaOH and otherwise the same condition as the optimal one for 2 h) with the 4.5 mg cm^{-3} sample, because the nanowires have similar lengths in the two samples but the 5.76 mg cm^{-3} sample has denser nanowires (Figure 2c,e), the 5.76 mg cm^{-3} sample has higher Young's modulus. In fact, for another sample synthesized under similar condition as the 5.76 mg cm^{-3} sample but with longer time (5 h), a density of 7.5 mg cm^{-3} (Figure S8, Supporting Information) was obtained. For this sample, Young's modulus of 1200 Pa and high mechanical strength of 26 kPa at 90% compression strain was observed (Figure S9, Supporting Information). We would like to point out that the samples we compared here have similar diameter distributions (70–90 nm), thus we anticipate the bulk samples mechanical properties are affected mostly by the density and length of the NWs in the samples. Figure 3d plots the relationship between relative Young's modulus and relative density for several low-density porous materials. The relative Young's modulus was found to scale with $(\rho\rho_s^{-1})^2$, indicating the highly efficient structure of our Cu aerosponge. When comparing the result of these samples with Cu nanowire aerogels from freeze casting,[33] the 7.5 mg cm^{-3} sample has Young's modulus 690 times higher than the loosely bounded Cu nanowire aerogel of 7.69 mg cm^{-3} (1.74 Pa).[33] Surprisingly, the value is also 7.5 times higher than the 160 Pa of the polyvinyl alcohol (PVA)–Cu nanowire composite aerogel with 9.6 mg cm^{-3},[38] even though PVA served as a glue for the Cu nanowire junction in the network. From these results, we found that the role played by the entanglement between the nanowires is significant, apparently longer nanowires give rise to higher Young's modulus for the bulk assembly.

The fluid wicking properties of the samples were also explored to elucidate the potential for use in fluid transport applications that rely on capillarity such as two-phase thermal management devices, where fluid transport to heated regions is critical to prevent dryout and device failure. **Figure 4**a shows a schematic of the experimental setup used to characterize the wicking behavior, where the samples brought into contact with a water reservoir at time $t = 0$, after which water wicked into the sample while high-speed video was recorded, with selected frames shown in Figure 4b (see the Experimental Methods section for details in the Supporting Information).

The propagation distance as a function of time for the CuNW aerosponges samples was quantified and plotted in Figure 4c, where the lower density (4.50 mg cm^{-3}) CuNW aerosponges demonstrated higher fluid wicking performance than the higher density sample (5.76 mg cm^{-3}). The 1D Darcy's law with gravitational effects included to account for liquid propagation against gravity over a distance greater than the capillary length

$$\frac{dx}{dt} = \frac{-\kappa}{\mu\phi}\left(\frac{-\Delta P_{cap}}{x} - \rho g\right) \quad (2)$$

was solved assuming a linear pressure gradient and used to plot the model curves shown in Figure 4c, where κ is permeability, μ is viscosity, ϕ is porosity, ΔP_{cap} is the driving capillary pressure, ρ is density, and g is the acceleration due to gravity. The capillary pressure was determined from the aerosponge fiber diameter d and the porosity with a commonly used method which considers the change in total surface energy as a given fluid volume propagates into the wicking structure, as shown in Section S3 in the Supporting Information.[25] The permeability of the wick was predicted from the fiber diameter and porosity with models in the literature for 3D randomly overlapping fibers, also detailed in the Supporting Information.[26,27] Therefore, the model curves only require the physical parameters μ, ρ, ϕ, g, and d, and as such are generated without the use of fitting parameters.

The model results showed good agreement with the wicking data for the CuNW aerosponges and supported the experimentally observed trend of increasing propagation rate with decreasing density. Additionally, a sintered copper wick sample prepared by sintering 10 μm copper powder (Sigma-Aldrich) at 850 °C with a resultant porosity of 0.52 was compared with the CuNW aerosponges. The model was also applied to the sintered wick and agreed well with the experimental results as well as with literature (the Supporting Information details the comparison of the sintered wick experimental data with the literature). The CuNW aerosponge samples exhibited excellent wicking

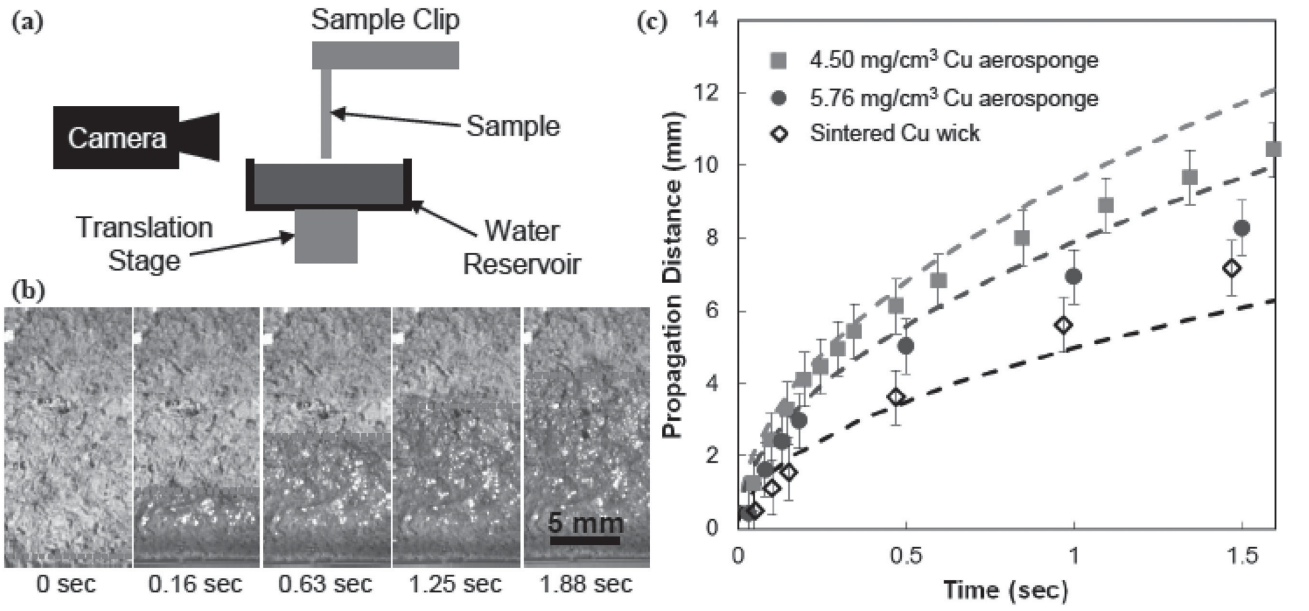

Figure 4. The copper aerosponge wicking properties were measured on a test apparatus a) comprised of a stationary sample and a water reservoir. The water reservoir was raised slowly until contact was made with the sample, at which point the wicking process was observed with a high speed camera and the propagation of the liquid front was quantified from the video b). The propagation distance is plotted against time for aerosponges with different densities as well as a sintered copper wick tested with the present experimental setup, along with models based on Darcy's law (dashed lines) c). The propagation rate for the copper aerosponges was observed to decrease for denser samples, with both of the copper aerosponges exhibiting better wicking performance as compared to the sintered copper wick.

behavior as compared to the sintered sample; the permeabilities of 2×10^{-11} m^2 (4.5 mg cm^{-3}) and 7×10^{-12} m^2 (5.76 mg cm^{-3}) are comparable to or higher than previously reported values for sintered wicks in the literature of 10^{-13}–10^{-11} m^2,[28–30] and much higher than the permeability of the experimentally fabricated sintered wick sample of 2×10^{-13} m^2. Sintered wicks are prevalent in many liquid transport and thermal management applications; thus, this comparison offers promise for use of CuNW aerosponges in heat pipes, particularly considering the potential reduction in materials required for heat pipe wick fabrication (CuNW aerosponges use as little as 0.1% of the copper required for sintered wicks) while maintaining liquid supply and therefore device cooling as indicated by the wicking performance. In addition, recent work has shown that pool boiling enhancement depends strongly on the wickability of the boiling surface, which is another potential application of the CuNW aerosponges fabricated in the present work.[31]

In conclusion, we developed a facile methodology to enable ultralight and highly porous metal nanowire aerosponges production from in situ nanowire hydrogel. The networks with interconnected metal nanowires were obtained by one-step metal nanowire synthesis without specific crosslinking agent. The density, porosity, and electrical and mechanical properties of the nanowire networks can be controlled by the initial concentration and reaction time and temperature. Superior properties such as high porosity, high electrical conductivities, mechanical robustness, and excellent water wicking efficiency allow these aerosponges to be used in many areas, such as heat sink, catalysis, or sensing, energy storage, etc., in this work we investigated particularly the heat exchange and found excellent performance from these one-step made aerosponges. We anticipate many more varieties of nanowire aerosponges can be produced via this methodology for various different applications in the future.

Supporting Information

Supporting Information is available from the Wiley Online Library or from the author.

Acknowledgements

The work was supported by the MIT Lincoln Laboratory Advanced Concepts Committee as well as from the Office of Naval Research (ONR) with Dr. Mark Spector as program manager. We also acknowledge the support from the National Science Foundation through the Major Research Instrumentation Grant for Rapid Response Research (MRI-RAPID) for the microgoniometer. S.M.J. acknowledges MIT Institute of Soldier Nanotechnologies (ISN) for the access of various instruments to carry out this work and the help from Dr. Sungwoo Yang. D.J.P. acknowledges funding received by the National Science Foundation Graduate Research Fellowship under Grant No. 1122374. Any opinion, findings, conclusions, or recommendations expressed in this material are those of the authors(s) and do not necessarily reflect the views of the National Science Foundation.

Received: September 28, 2015
Revised: October 30, 2015
Published online: December 4, 2015

[1] R. Menzel, S. Barg, M. Miranda, D. B. Anthony, S. M. Bawaked, M. Mokhtar, S. A. Al-Thabaiti, S. N. Basahel, E. Saiz, M. S. P. Shaffer, *Adv. Funct. Mater.* **2015**, *25*, 28.
[2] K. W. Oh, D. K. Kim, S. H. Kim, *Fibers Polym.* **2009**, *10*, 731.

[3] a) N. H. Sing, U. Schubert, *Angew. Chem.* **1998**, *110*, 22; b) N. H. Sing, U. Schubert, *Angew. Chem. Int. Ed.* **1998**, *37*, 22.
[4] B. C. H. Steele, A. Heinzel, *Nature* **2001**, *414*, 345.
[5] Y. Chen, K. C. Ng, W. Yan, Y. Tang, W. Cheng, *RSC Adv.* **2011**, *1*, 1265.
[6] S. L. Brock, I. U. Arachchige, K. K. Kalebaila, *Comm. Inorg. Chem.* **2006**, *27*, 103.
[7] S. Bag, P. N. Trikalitis, P. J. Chupas, G. S. Armatas, M. G. Kanatzidis, *Science* **2007**, *317*, 490.
[8] S. Bag, M. G. Kanatzidis, *J. Am. Chem. Soc.* **2008**, *130*, 8366.
[9] J. L. Mohanan, I. U. Arachchige, S. L. Brock, *Science* **2005**, *307*, 397.
[10] S. L. Brock, I. U. Arachchige, J. L. Mohanan, *Science* **2005**, *307*, 397.
[11] I. U. Arachchige, S. L. Brock, *J. Am. Chem. Soc.* **2006**, *128*, 7964.
[12] S. L. Brock, K. Senevirathne, *J. Solid State Chem.* **2008**, *181*, 1552.
[13] J. P. Boilot, P. Larregaray, K. Lahlil, T. Gacoin, *J. Phys. Chem. B* **2001**, *105*, 228.
[14] B. C. Tappan, S. A. Steiner, E. P. Luther, *Angew. Chem., Int. Ed.* **2010**, *49*, 4544.
[15] A. Varma, A. S. Rogachev, A. S. Mukasyan, S. Hwang, *Adv. Chem. Eng.* **1998**, *24*, 79.
[16] P. Erri, J. Nader, A. Varma, *Adv. Mater.* **2008**, *20*, 1243.
[17] E. M. Hunt, M. L. Pantoya, R. J. Jouet, *Intermetallics* **2006**, *14*, 620.
[18] D. E. Chavez, M. A. Hiskey, D. L. Naud, *J. Pyrotech.* **1999**, *10*, 17.
[19] T. A. Schaedler, A. J. Jacobsen, A. Torrents, A. E. Sorensen, J. Lian, J. R. Greer, L. Valdevit, W. B. Carter, *Science* **2011**, *334*, 962.
[20] D. Wang, H. Luo, R. Kou, M. P. Gil, S. Xiao, V. O. Golub, Z. Yang, C. J. Brinker, Y. Lu, *Angew. Chem., Int. Ed.* **2004**, *43*, 6169.
[21] J. T. Korhonen, P. Hiekkataipale, J. Malm, M. Karppinen, O. Ikkala, R. H. A. Ras, *ACS Nano* **2011**, *5*, 1967.
[22] S. M. Jung, H. Y. Jung, M. S. Dresselhaus, Y. J. Jung, J. Kong, *Sci. Rep.* **2012**, *2*, 849.
[23] S. M. Jung, H. Y. Jung, W. Feng, M. S. Dresselhaus, J. Kong, *Nano Lett.* **2014**, *14*, 1810.
[24] W. He, G. Li, S. Zhang, Y. Wei, Q. Li, X. Zhang, *ACS Nano* **2015**, *9*, 4244.
[25] R. Xiao, R. Enright, E. N. Wang, *Langmuir* **2010**, *26*, 15070.
[26] M. M. Tomadakis, T. J. Robertson, *J. Compos. Mater.* **2005**, *39*, 163.
[27] G. W. Jackson, D. F. James, *Can. J. Chem. Eng.* **1986**, *64*, 364.
[28] M. Annamalai, S. Dhanabal, presented at the *International Refrigeration and Air Conditioning Conference*, Purdue University, Purdue e-Pubs, West Lafayette, IN, July **2012**.
[29] S. Samanta, B. Sharma, P. Das, A. Lohar, *Frontiers Heat Pipes* **2012**, *2,* 043001.
[30] W. W. Wits, J. H. Mannak, R. Legtenberg, presented at *The 5th European Thermal-Sciences Conference*, Eindhoven, Netherlands, May **2008**.
[31] M. M. Rahman, E. Olceroglu, M. McCarthy, *Langmuir* **2014**, *30*, 11225.
[32] Y. Chang, M. L. Lye, H. C. Zeng, *Langmuir* **2005**, *21*, 3746.
[33] Y. Tang, K. L. Yeo, Y. Chen, L. W. Yap, W. Xiong, W. Cheng, *J. Mater. Chem. A* **2013**, *1*, 6723.
[34] a) B. Berkowitz, R. Knight, *J. Stat. Phys.* **1995**, *80*, 1415; b) A. Aharony, in *Directions in Condensed Matter Physics* (Eds: G. Grinstein, G. Mazenko), World Scientific, Singapore, **1986**, pp. 1–50.
[35] M. Sahimi, B. D Hughes, L. E. Scriven, H. T. Davis, *J. Phys. C: Solid State Phys.* **1983**, *16*, L5214527.
[36] a) I. Balberg, *Phys. Rev. B* **1988**, *33*, 3618; b) I. Balberg, N. Binenbaum, *Phys. Rev. A* **1985**, *31*, 1222; c) K. S. Mendelson, M. H. Cohen, *Geophysics* **1982**, *47*, 257.
[37] R. M. Mutiso, M. C. Sherrott, A. R. Rathmell, B. J. Wiley, K. I. Winey, *ACS Nano* **2013**, *7*, 7654.
[38] Y. Tang, S. Gong, Y. Chen, L. W. Yap, W. Cheng, *ACS Nano* **2014**, *8*, 5707.

Submitted to ADVANCED MATERIALS

Supporting Information

for *Adv. Mater.*, DOI: 10.1002/adma. 201504774

Porous Cu nanowire aerosponge from one step assembly and their applications in heat dissipation

Sung Mi Jung, Daniel John Preston, Hyun Young Jung, Zhengtao Deng, Evelyn N. Wang, Jing Kong*

S1. Experimental Methods

Copper nanowire (CuNW) hydrogel/aerosponge production: For Cu nanowire synthesis, the precursor materials were composed of sodium hydroxide (NaOH, 13-18M), copper sulfate (CuSO4, 0.5-1.5M), ethylenediamine (EDA, 99 wt %), and hydrazine (35 wt %) in a ratio of 2000:2:3:0.25, and the precursor suspension was initially dispersed by ultra-sonication and add to a glass vessel and then, the sealed glass vessel was heated in oil bath at 50-85 °C for 0 min to 15 h of reaction time. During the Cu nanowire synthesis process, the Cu nanowires grow out from the precursor suspension and the length and concentration of nanowires increased and the grown nanowires were interconnected each other and then form a continuous Cu nanowire hydrogel network at gel formation concentration. The principle of gel formation is the same as our previous work[1], however, the gel formation process should be distinguished with the previous work[1], which the Cu nanowires gel network was assembled from physical bonding of nanowires by vander-Waals force while the dilute nanowire suspension transforms into concentrated suspension by evaporation of the solvent at transition regime between semi-dilute and

isotropic concentrated regime (gel formation concentration = reciprocal of aspect ratio of nanowire). The in-situ Cu nanowire hydrogel was washed in a water-hydrazine solution to prevent oxidation and frozen at 80 oC. After that, the in-situ nanowire hydrogels were freezing dried into aerosponges to retain the original gel volume.

Experimental fluid propagation measurement: The copper aerosponge wicking properties were determined by measuring the propagation of fluid through the samples as a function of time. The test apparatus was comprised of a stationary sample and a fluid reservoir which was filled with deionized water. The water reservoir was raised slowly (less than 0.1 mm/sec) until contact was made with the sample, at which point the wicking process was observed with a high speed camera (Vision Research Phantom 7.1). The propagation of the liquid front was quantified by post-processing the high speed videos using imaging analysis software.

Characterization: Scanning electron microscopy (JEOL 6700F) was used to find the morphology and the porosities of the aerosponge networks. Transmission electron microscopy (TEM, JEOL 2010F) was used to investigate the diameters and structures of the Cu nanowires. X-ray diffraction (Rigaku RU300, CuKa radiation) analysis was used to obtain the crystallinities of Cu nanowires. The krypton adsorption isotherms for surface area of the aerosponges were measured at 77 K on a Micromeritics ASAP 2010 system. Before measurement, the samples were degassed at 423 K under vacuum ($<10^{-4}$ mbar) for several hours. The surface areas of the aerosponges were computed using the

Brunauer-Ennett-Teller (BET) method based on the multimolecular layer adsorption model. MTS Nano Instruments model Nano-UTM were used for compression testing of the Cu nanowire aerosponges.

S2. Supplementary Data

Structural characterization of CuNW aerosponges

The crystallinity of the synthesized CuNW aerosponges were further characterized by X-ray diffraction (XRD) (Fig. S1). X-ray photoelectron spectroscopy (XPS) results for our Cu nanowire aerosponges are reported in Figure S2. Cuprite Cu_2O (about 7% among total surface copper) was found on the wire surfaces, on the basis of an analysis for the binding energies of Cu $2p_{3/2}$ (932.4 eV for Cu^0 and 932.2 eV for Cu+; reference C 1s was set at 284.7 eV) [1] and O 1s (530.2 eVfor the anion O^{2-} in the cuprite) [2]. The surface area of the sample in Figure 1e was characterized by the Brunauer-Ennett-Teller (BET) method to be 12 m^2g^{-1} (Fig. S3).

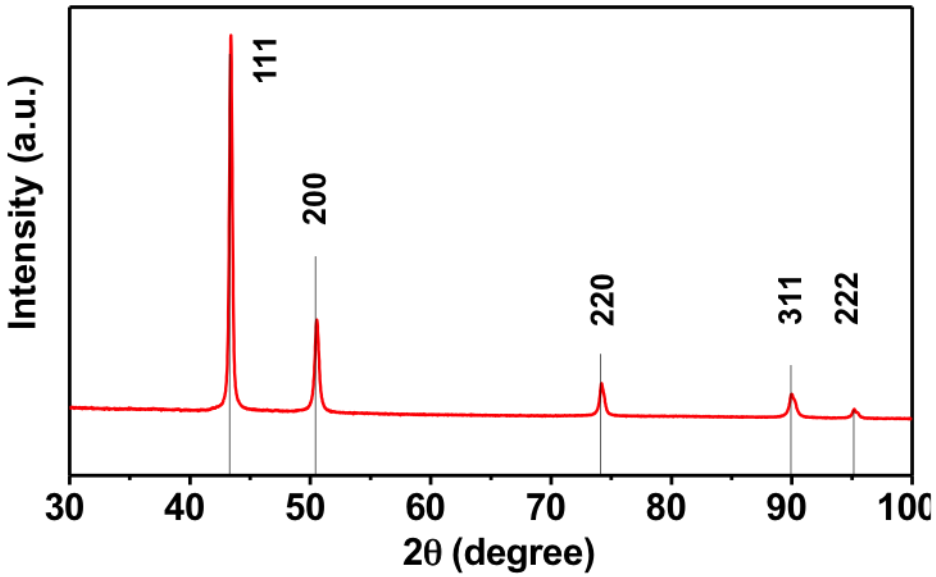

Figure S1. XRD patterns of CuNW aerosponges produced at 16M NaOH, 1M $CuSO_4$, 80^0C, and 2h. XRD patterns show that CuNW aerosponges have a face-centered cubic (fcc) structure (SG: Fm3m; JCPDS card no. 04-0836), and the lattice constant of this cubic phase ao is equal to 3.615 Å.[4]

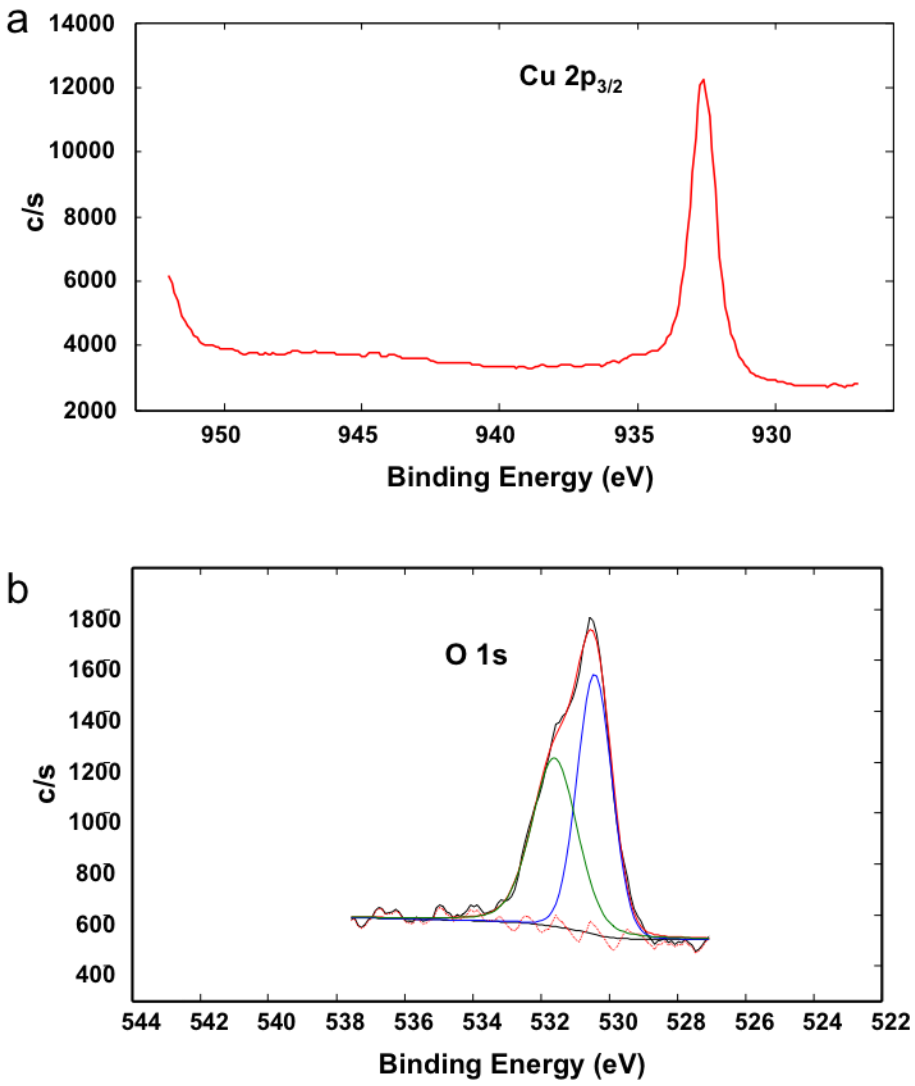

Figure S2. (a) and (b) XPS spectra of Cu $2p_{3/2}$ and O 1s photoelectrons of CuNW aerosponges produced at 16M NaOH, 1M $CuSO_4$, 80^0C, and 2h.

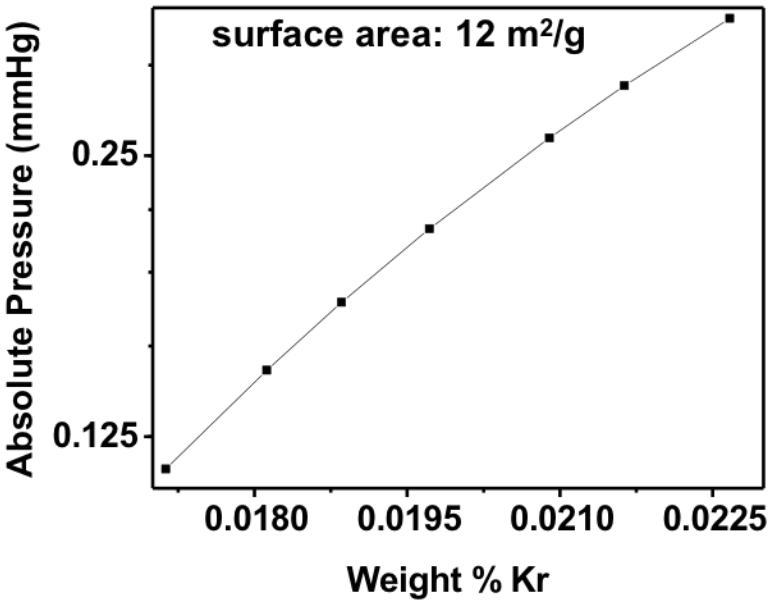

Figure. S3. The surface area (12 m^2/g) of the CuNW aerosponge produced at 18M NaOH, 1M $CuSO_4$, 80^0C, and 2h measured by the Brunauer-Ennett-Teller (BET) method.

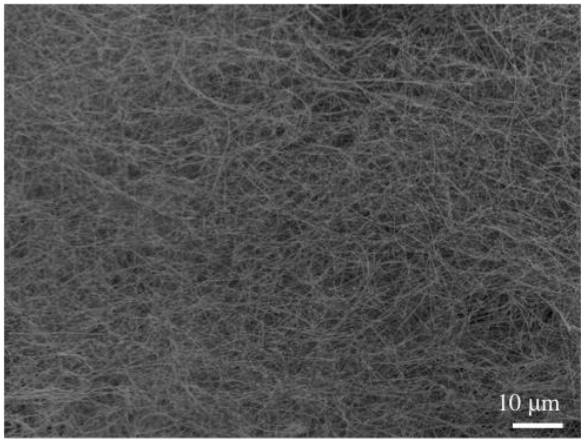

Figure S4. SEM image of ultralong CuNW aerosponge produced at 16M NaOH, 1M $CuSO_4$, 80^{o}C for 2 hr.

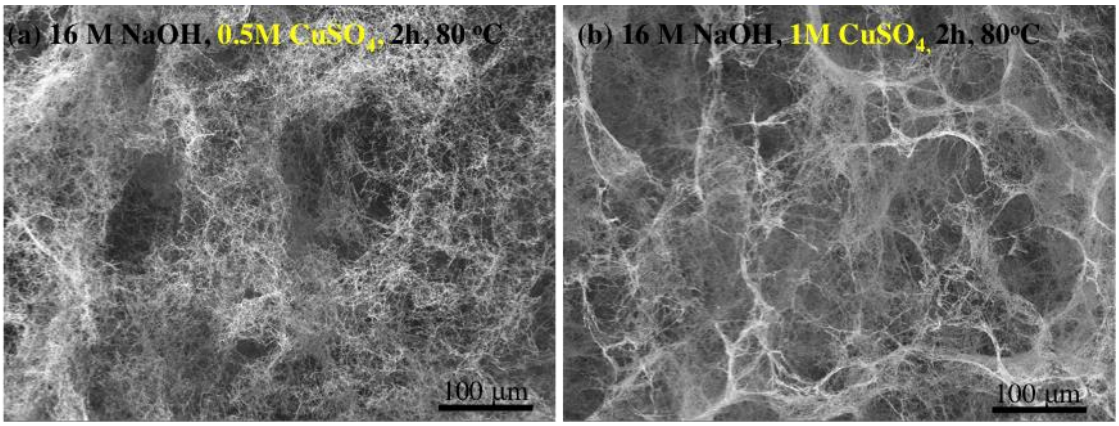

Figure S5. Low magnification SEM images of highly porous CuNW aerosponges produced at (a) 16M NaOH, 0.5M $CuSO_4$, 80^{o}C, 2 hr and (b) 16M NaOH, 1M $CuSO_4$, 80^{o}C, 2 hr.

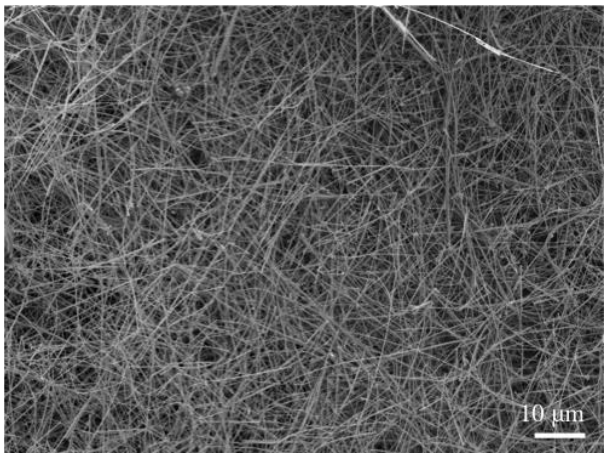

Figure S6. SEM image of the CuNW aerosponge produced at 18M NaOH, 1M $CuSO_4$, 80^oC for 5 hr.

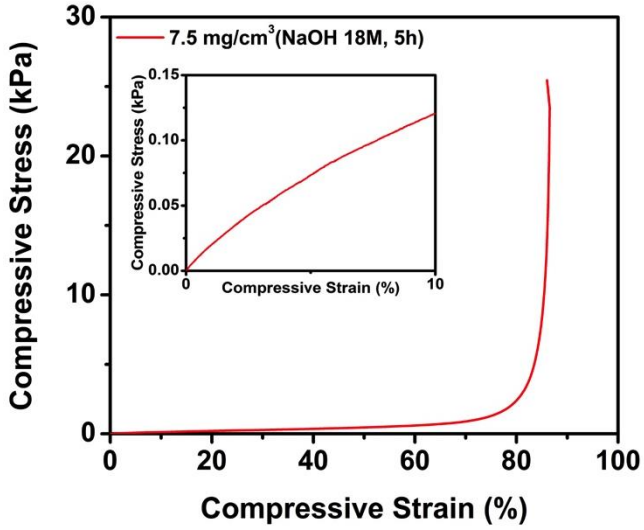

Figure S7. Compressive stress/strain test for the aerosponges with different densities of 7.5 mg/cm^3 (NaOH 18M, 1M $CuSO_4$, 5h, 80 ^0C).

S3. Wicking Fluid Propagation Model

Darcy's Law with Gravitational Effects

The form of Darcy's law with gravitational effects was used for the wicking model since the wicking drew fluid against gravity over a distance significantly larger than the capillary length:

$$\frac{dx}{dt} = \frac{-\kappa}{\mu\varphi}\left(\frac{-\Delta P_{cap}}{x} - \rho g\right) \tag{S1}$$

where the derivative of the propagation distrance, x, with respect to time, t, is shown as a function of the viscosity (μ) and density (ρ) as well as the wick property of porosity (φ) which can be determined from the wick density and the gravitational acceleration (g). The driving capillary pressure (ΔP_{cap}) and permeability of the wick (κ) are determined from the known wick porosity and wick fiber diameter as well as the contact angle of water on the wick material (copper) and the water-vapor interfacial tension as demonstrated in the following two subsections. The solution can be found explicitly for time as a function of the distance over which the fluid has propagated (solving for propagation distance as a function of time requires implementation of the Lambert W function):

$$t = \frac{Aln(A - Bx) + Bx - Aln(A)}{(B)^2}, \qquad A = \frac{\kappa \Delta P_{cap}}{\mu\varphi}, \qquad B = \frac{\kappa\rho g}{\mu\varphi} \tag{S2}$$

Therefore, from only the physical parameters μ, ρ, φ, g, and the aerosponge fiber dimension d (used to determine capillary pressure and permeability as shown in the following two sections), the model curves shown in Figure 4 in the manuscript are generated without the use of fitting parameters.

Calculation of the Capillary Pressure

The capillary pressure was calculated based on a commonly used method in the literature which considers the change in total surface energy as a given fluid volume propagates into the wicking structure [5]:

$$\Delta P_{cap} = \frac{-\Delta E}{\Delta V} \tag{S3}$$

For a wicking structure mounted to a solid substrate on once face (for support) and exposed to air on the other face (for imaging), with a thickness *h* between faces and liquid propagation occurring parallel to the plane of the faces, the overall change in energy as a unit area of the faces and structure is wetted is:

$$\Delta E = (\gamma_{LV} + \gamma_{SL} - \gamma_{SV})(1m^2) + (\gamma_{SL} - \gamma_{SV})(A/V)_{wick}\Delta V \tag{S4}$$

where the corresponding change in wetted volume is:

$$\Delta V = h(1m^2) \tag{S5}$$

The wick area per unit volume of the samples studied in the present work was no less than 32,000 m^2/m^3. Therefore, since all of the interfacial surface energies are on the same order of magnitude, the wick suface wetting energy term dominates when the following criteria is met:

$$\frac{(A/V)_{wick}\Delta V}{(1m^2)} = (A/V)_{wick}h \gg 1 \tag{S6}$$

which is equivalent to:

$$h \gg 30\ \mu m \tag{S7}$$

The thickness *h* of the wicks in the present study were approximately 2 mm, which is much greater than 30 μm. Therefore, the contributions to the change in energy from wetting of the wick faces can be neglected, and the capillary pressure can be written as:

$$\Delta P_{cap} = -(\gamma_{SL} - \gamma_{SV})(A/V)_{wick} \tag{S8}$$

This can be further simplified by substituting Young's equation:

$$\Delta P_{cap} = (\gamma_{LV}\cos(\theta))(A/V)_{wick} \quad \text{(S9)}$$

where the contact interfacial tension for the liquid-vapor interface γ_{LV} and the contact angle θ are known (θ approaches zero for water on cleaned copper, resulting in $\cos(\theta) \approx 1$). Finally, the parameter $(A/V)_{wick}$ must be determined from the known quantites of wick density and wick fiber diameter. The cross-sectional area A_{xc} and circumference C of a wick fiber are obtained from the fiber diameter, and the volume fraction of the wick (V_{Cu}/V) is calculated as the wick density divided by the density of the wick material (copper). Then, the total fiber length per unit volume of wick is $l = (V_{Cu}/V) / A_{xc}$ and the total wick surface area per unit volume of wick is $(A/V)_{wick} = Cl$.

Prediction of the Permeability

The permeability of the wick was predicted from models reported in the literature. For 3-D randomly overlapping fibers, the permeability is proposed by Tomadakis and Robertson based on Archie's law to be [6]:

$$\kappa = r^2 \frac{\varepsilon}{8\ln^2(\varepsilon)} \frac{(\varepsilon - \varepsilon_p)^{\alpha+2}}{(1-\varepsilon_p)^{\alpha}[(\alpha+1)\varepsilon - \varepsilon_p]^2} \quad \text{(S10)}$$

where r is the fiber radius, ε is the porosity, and the parameters $\varepsilon_p = 0.037$ and $\alpha = 0.661$ were used for 3-D randomly overlapping fibers. An alternate correlation for 3-D randomly overlapping fibers proposed by Jackson and James was also used [7]:

$$\kappa = r^2 \frac{3}{20\varphi}(-\ln(\varphi) - 0.931 + O(\ln(\varphi)^{-1})) \quad \text{(S11)}$$

where φ is the solid volume fraction. The value for wick permeability used in the model was taken as the gemoetric mean of these two predictions.

Capillary Pressure and Permeability Values

The capillary pressure and permeability values calucalted from the above equations and used in the Darcy's law solution to generate the model curves presented in Figure 4 are documented in Table S1 along with the characteristic wire radius or sinter particle size and the density:

Table S1. Capillary pressure and permeability for copper aerosponges and sintered wick.

Sample (density)	**Char. Dimension**	**Permeability**	**Cap. Pressure**
Cu aerosponge (4.50 mg/cm^3)	75 nm	2.1 x 10^{-11} m^2	2.3 kPa
Cu aerosponge (5.76 mg/cm^3)	75 nm	6.9 x 10^{-12} m^2	4.6 kPa
Sintered Cu wick (4.21 g/cm^3)	5 μm	2.4 x 10^{-13} m^2	27.1 kPa

Comparison with Literature

The present experimental results for the sintered copper wick were compared to literature which provided data for sintered copper wick with a comparable density (6.1 g/cm^3). The present work was in good agreement with the literature, as shown in Figure S8 where the propagation in the literature sintered wick was predicted with the provided permeability and capillary pressure input into the the Darcy's law solution presented in Equation S2.

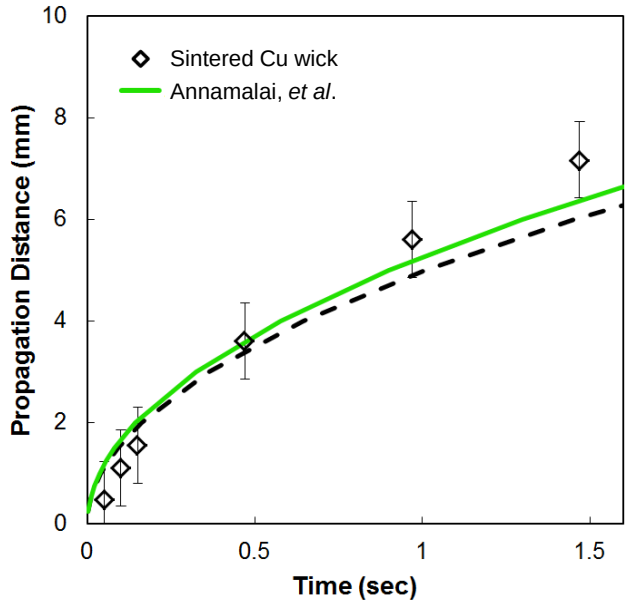

Figure S8. The propagation distance is plotted against time for the sintered copper wick tested with the present experimental setup, as well as the model for the sintered wick based on the calculated permeability and capillaty pressure (black dashed curve). A model curve for a sintered copper wick based on data from prior work (permeability κ = 9.15 x 10^{-13} m^2, capillary pressure ΔP_{cap} = 7.79 kPa from reported pore size of 18.5 μm and porosity 0.32) [8] is presented for comparison, with good agreement to the present experimental results.

Supporting Information References

[1] J. P. Espino´s, J. Morales, A. Barranco, A. Caballero, J. P. Holgado, A. R. Gonza´ lez-Elipe, J. Phys. Chem. B 2002, *106*, 6921.

[2] E. McCafferty, J. P. Wightman, Surf. Interface Anal. 1998, *26*, 549.

[3] H. Perez, P. Navarro, G. Torres, O. Sanz, M. Montes, Catal. Today 2013, *212*, 149.

[4] Swanson, Tatge., Natl. Bur. Stand. (U. S.), Circ. 539, I, 15, (1953).

[5] Xiao, R.; Enright, R.; Wang, E. N., Prediction and Optimization of Liquid Propagation in Micropillar Arrays. Langmuir 2010, 26 (19), 15070-15075.

[6] Tomadakis, M. M.; Robertson, T. J., Viscous permeability of random fiber structures: Comparison of electrical and diffusional estimates with experimental and analytical results. J Compos Mater 2005, 39 (2), 163-188.

[7] Jackson, G. W.; James, D. F., The Permeability of Fibrous Porous-Media. Can J Chem Eng 1986, 64 (3), 364-374.

[8] M. Annamalai, S. Dhanabal, In Experimental Studies On Porous Wick Flat Plate Heat Pipe, International Refrigeration and Air Conditioning Conference, Purdue University, West Lafayette, Indiana, July 12-15; Purdue e-Pubs: Purdue University, West Lafayette, Indiana, 2010